ARL-TR-9287 ● SEP 2021

DEVCOM ARMY RESEARCH LABORATORY

Comparison of Aeroprediction Methods for Guided Munitions

by Justin L Paul, Joseph D Vasile, and James DeSpirito

NOTICES

Disclaimers

The findings in this report are not to be construed as an official Department of the Army position unless so designated by other authorized documents.

Citation of manufacturer's or trade names does not constitute an official endorsement or approval of the use thereof.

Destroy this report when it is no longer needed. Do not return it to the originator.

ARL-TR-9287 ● SEP 2021

Comparison of Aeroprediction Methods for Guided Munitions

Justin L Paul, Joseph D Vasile, and James DeSpirito
Weapons and Materials Research Directorate,
DEVCOM Army Research Laboratory

REPORT DOCUMENTATION PAGE

Form Approved
OMB No. 0704-0188

1. REPORT DATE *(DD-MM-YYYY)*	2. REPORT TYPE	3. DATES COVERED (From - To)
September 2021	Technical Report	1 October 2019–31 July 2021

4. TITLE AND SUBTITLE
Comparison of Aeroprediction Methods for Guided Munitions

5a. CONTRACT NUMBER

5b. GRANT NUMBER

5c. PROGRAM ELEMENT NUMBER

6. AUTHOR(S)
Justin L Paul, Joseph D Vasile, and James DeSpirito

5d. PROJECT NUMBER

5e. TASK NUMBER

5f. WORK UNIT NUMBER

7. PERFORMING ORGANIZATION NAME(S) AND ADDRESS(ES)
DEVCOM Army Research Laboratory
ATTN: FCDD-RLW-WD
Aberdeen Proving Ground, MD 21005

8. PERFORMING ORGANIZATION REPORT NUMBER
ARL-TR-9287

9. SPONSORING/MONITORING AGENCY NAME(S) AND ADDRESS(ES)

10. SPONSOR/MONITOR'S ACRONYM(S)

11. SPONSOR/MONITOR'S REPORT NUMBER(S)

12. DISTRIBUTION/AVAILABILITY STATEMENT
Approved for public release: distribution unlimited.

13. SUPPLEMENTARY NOTES
ORCID IDs: Justin Paul 0000–0003–4133–7585; Joseph Vasile, 0000–0003–3812–6277

14. ABSTRACT
Several aeroprediction methodologies were used to evaluate four munition configurations: a generic canard-controlled, subsonic projectile; a long strake-tail missile; a generic ogive-body-tail supersonic missile; and a generic high-speed munition. Numerous flight conditions of angle of attack, roll angle, and Mach number were investigated. The aeroprediction methodologies included inviscid and viscous computational fluid dynamics solvers and a semi-empirical aerodynamic design code. The results were evaluated for agreement with each other and with respect to experimental data in order to better determine the use cases and applications of these methodologies. The range of results revealed notable differences in how the methodologies handle unique flow features that occur for different geometries at different flow conditions.

15. SUBJECT TERMS
guided munitions, aerodynamics, computational fluid dynamics, CFD, aeroprediction, comparison

16. SECURITY CLASSIFICATION OF:			17. LIMITATION OF ABSTRACT	18. NUMBER OF PAGES	19a. NAME OF RESPONSIBLE PERSON
a. REPORT	b. ABSTRACT	c. THIS PAGE			Justin L Paul
Unclassified	Unclassified	Unclassified	UU	44	19b. TELEPHONE NUMBER (Include area code) (410) 306-0797

Contents

List of Figures

List of Tables

Acknowledgments

The authors thank Mr Joshua Doyle and Mr Christopher Rosema, US DEVCOM Aviation and Missile Center, for their help and discussions regarding Missile DATCOM fundamentals and techniques. This work was supported in part by a grant of high-performance computing time from the US Department of Defense (DOD) High Performance Computing Modernization program at the US Army Research Laboratory DOD Supercomputing Resource Center (DSRC), Aberdeen Proving Ground, Maryland, and the US Army Engineer Research and Development Center DSRC, Vicksburg, Mississippi.

1. Introduction

Accurate prediction of aerodynamic coefficients is vital to the development of accurate aerodynamic models that can be used in design and analysis. The advent of guided munitions has at times put a strain on the usefulness of low-fidelity analysis tools, such as those based on semi-empirical methods. In design and analysis applications, accurate predictions now require "production-level" computational fluid dynamics (CFD)—the exact scale of which may differ among organizations. It is important to know the level of accuracy for all of these methodologies and any complications they may encounter given an arbitrary vehicle configuration at all flight regimes of interest.

The purpose of this study is to gain insight and further understand the limitations of lower-fidelity codes in accurately predicting the aerodynamic coefficients for guided munitions. Common low-order (semi-empirical), intermediate-order (inviscid CFD), and high-fidelity (Navier–Stokes CFD) prediction tools are compared. The examples studied explore different flow regimes as well as control strategies that assess the accuracy of lower-fidelity codes. Some of the unknown aerodynamic effects that were investigated are 1) the accuracy of lower-fidelity codes at subsonic speeds, 2) the accuracy in predicting the adverse flow interactions present for tandem control munitions (e.g., adverse roll moment in canard-tail or wing-tail configurations), 3) the accuracy in predicting the aerodynamic coefficients for complex shaped munitions (e.g., strake configurations), and 4) the accuracy associated with modeling control-surface deflections. The comparison of aeroprediction methods provides greater awareness in the capabilities of lower-fidelity codes, as well as improve confidence in predicting aerodynamic coefficients of guided munitions. Citations of references for each example are provided for additional details.

2. Computational Methodology

2.1 Semi-Empirical Methods

Missile DATCOM[1] is an engineering-level prediction code for estimating the aerodynamic stability and control characteristics of conventional missile configurations. It uses both theoretical and empirical methods to encompass the entire speed regime from subsonic to hypersonic flight. In previous versions of Missile DATCOM, predictions of vortex–fin interactions (i.e., shedding vortices from upstream control surfaces impacting downstream tail fins) were quite poor due to insufficient modeling capabilities. However, more recently, the US Army

Combat Capabilities Development Command Aviation and Missile Center has made significant improvements to the vortex modeling capabilities, including improved fin-shed and body-shed vortex models.[2,3] These improvements allow for better predictions of complex flow interactions, such as vortex-induced flow phenomena (e.g., induced roll for canard-controlled projectiles). The Graphical User Interface MissileLab (version 9.0.63)[4] was employed to create input files and execute Missile DATCOM. Using Missile DATCOM, one can get answers within seconds on a commercial laptop.

2.2 Euler (Inviscid) Computational Fluid Dynamics

NASA's Cart3D is an inviscid CFD package for aerodynamic design and analysis. Cart3D provides capabilities for surface modeling and intersection, mesh generation, flow simulation, and postprocessing.[5,6] The mesh generation software with the Cart3D package produces Cartesian meshes for arbitrarily complex, watertight geometries. The mesh generation process automatically increases the fidelity of domains near small features and curvatures to better resolve flow features near the surface. The option also exists to create higher-resolution areas in the wake of the body. Adjoint-based mesh adaption is also available to refine the mesh based on the flow solution. Aerodynamic coefficients for a given flight condition (i.e., Mach number and aerodynamic angles) are computed in several (5–10) minutes on a desktop workstation or a single node on a High Performance Computing (HPC) machine.

2.3 Navier–Stokes Computational Fluid Dynamics

Two Reynolds–Averaged Navier–Stokes (RANS) solvers were used in this study, CFD^{++} and Kestrel. RANS solutions typically took a few (2–5) hours on HPC machines using 50,000–100,000 cells per core.

1. CFD^{++}

CFD^{++}[7] is a 3D compressible solver in which the RANS equations are solved using a finite-volume method. A point-implicit time-integration scheme with local time-stepping, defined by the Courant–Friedrichs–Lewy (CFL) number, was used to advance the solution toward steady state. The multigrid W-cycle method with a maximum of 4 cycles and a maximum of 20 grid levels was used to accelerate convergence. The inviscid flux function was a second-order, upwind scheme using a Harten–Lax–van Leer–contact Riemann solver and a multidimensional Total-Variation-Diminishing minmod flux limiter. Menter's Shear–Stress Transport (SST) model[8] was used for turbulence closure.

2. Kestrel

Kestrel was developed under the US Department of Defense (DOD) High Performance Computing Modernization Program initiative to improve DOD acquisition programs through use of computational science and engineering tools.[9] The result of the initiative is called the Computational Research and Engineering Acquisition Tools and Environments (CREATE) Program, which was established in 2008. The air vehicle portion of CREATE is referred to as CREATE-AV[10] and the high-fidelity, fixed-wing vehicle simulation tool is called Kestrel.[11,12] In addition to the unstructured mesh solver, KCFD software includes a Cartesian-mesh solver used for dual-mesh simulations.[13,14] The Cartesian solver, SAMAIR, includes solution adaptive mesh refinement (AMR) and is connected to the near-body (NB) mesh via overset-mesh methodology.

KCFD is a finite-volume, cell-centered, unstructured flow solver for 2D and 3D discretized domains. Meshes can be composed of tetrahedron, prism, pyramid, and hexahedron cells in 3D, or triangles and quadrilaterals in 2D. KCFD employs the Method of Lines using a typical Godunov scheme to compute the spatial residual with second-order accuracy. Various exact and approximate Riemann schemes to compute the fluxes at each element face and up to second-order accuracy is achieved via a subiterative point-implicit scheme. The Spalart–Allmaras one-equation model[14] and Menter's baseline and SST two-equation[8] turbulence models are also available.

3. Results

One objective of this study was to evaluate the performance of the prediction tools on different configurations and in different Mach number regimes. Some configurations were chosen for either subsonic only or supersonic only flight. In addition, configurations were also considered that operated in the subsonic, transonic, and supersonic flight regimes. Four configurations are presented: the Generic Canard-Controlled Subsonic Projectile, the NASA Strake-Tail Missile, the US Air Force Finner (AFF), and DEVCOM Army Research Laboratory's Laboratory Technology Vehicle (LTV).

3.1 Generic Canard-Controlled Subsonic Projectile

A relatively short length-to-diameter-ratio projectile with two canards deflected for either pitch or roll at subsonic speeds was investigated. Two tail-fin sets, 4-fin and 8-fin, each at two rotated orientations, were included for a total of four configurations. This configuration suffered from vortex–fin interactions that induced adverse roll moment on the tail fins.[15]

A schematic of a nominal body–fin–canard configuration used in the current investigation is presented in Fig. 1. The projectile has a 40-mm diameter (d) with a length (L) of 180 mm corresponding to a length-to-diameter ratio of 4.5. The center of gravity of the projectile was set to the midpoint along the longitudinal body axis (i.e., 90 mm forward of the base). The projectile has a hemispherical nose (radius of 20 mm) and a 7° boattail beginning 10 mm forward of the base. All projectiles considered contain a set of two unswept rectangular flat-plate canards with a chord of 15 mm, a semi-span of 40 mm, and a thickness of 0.5 mm, with the quarter chord axis located 33.75 mm aft of the nose of the projectile. The overall dimensions of the canards were held constant throughout the study. The canard control-surface dimensions were selected based on a previous study that optimized the lift-to-drag of the vehicle when the canards were deflected for positive pitch at 5° (i.e., $\delta = 5°$).[16] All canard deflections were rotated about the quarter chord. The goal of the study is to investigate the effect of tail-fin geometry, both size and roll (ϕ) orientation, on the aerodynamic performance of the overall projectile when canards are deflected for both positive pitch and positive ϕ. Each tail-fin set was placed at the rear of the projectile, with the trailing edge of the fins set flush to the base of the projectile. All tail-fin sets studied are rectangular flat plates with a chord of 20 mm and a thickness of 0.5 mm. The semi-span values for the 4- and 8-fin configurations were 60 and 45.5 mm, respectively. Each tail-fin set configuration consist of two ϕ orientations relative to the horizontal canards, a plus ("+") and a cross ("x") variant. The 4- and 8-fin cross variants are rotated 45° and 22.5° off plane, respectively. More description and details of the projectiles and investigation can be found in Vasile.[15]

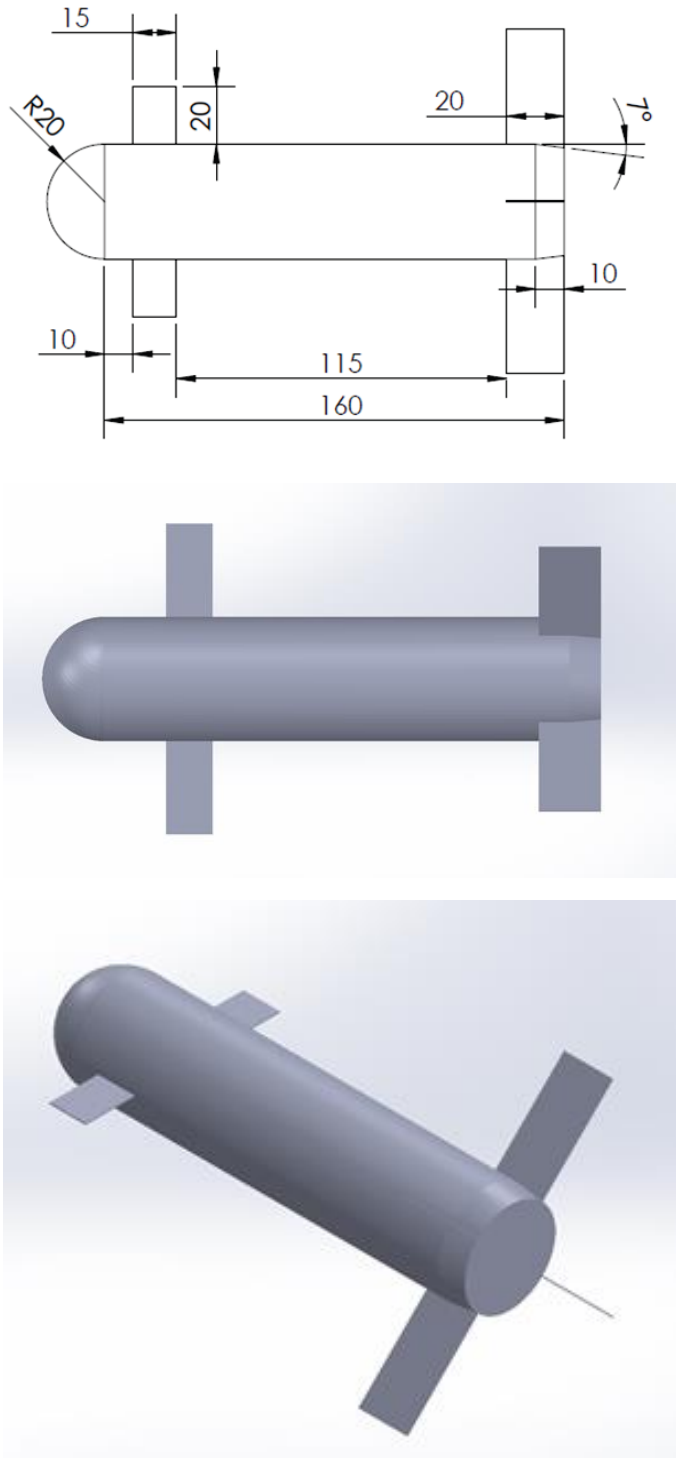

Fig. 1 Schematic and geometric model of body–fin–canard projectile

Multiple aeroprediction codes with varying fidelity were used to characterize the projectile. The semi-empirical aeroprediction code Missile DATCOM, the inviscid analysis package Cart3D (flowCart), and the Navier–Stokes CFD flow solver

Kestrel (KCFD) were used. Simulation results are compared with experimental wind tunnel (WT) or aeroballistics range data when available.

For the Cart3D simulations, the computational domain extended approximately 14 projectile lengths in all directions from the center of the projectile, and the smallest typical grid size for the domain was approximately 0.6 × 0.6 × 0.6 mm. Mesh density regions were defined to refine the mesh near the surface as well as in the wake region to help resolve flow structures. These regions are further refined during the flow solution via the AMR. The computational domain consisted of approximately 6 million Cartesian cells. Once the mesh is generated, the flow solver (flowCart) exploits the features of the Cartesian grid to quickly compute the flow field and aerodynamic forces and moments experienced by the configuration. The Cart3D analysis package provides only inviscid aerodynamic coefficients.

For the Navier–Stokes CFD flow-solver Kestrel, an NB unstructured and Cartesian outer-body mesh that generated via the AMR capability within SAMAIR was implemented (Fig. 2). The NB mesh was generated using the Capstone (version 8.0.3)[17,18] mesh generator, which was also developed under the CREATE program. The NB mesh extends to about 5 mm (0.3 canard chord lengths) from the projectile surface and consists of about 13.9 million cells. The NB mesh was designed for eventual use using the time-accurate RANS/large eddy simulation technique, so it is somewhat denser in general than may be typically used for a straight RANS simulation. The first cell edge was located 1.5×10^{-3} mm from the solid wall, resulting in $y^+ \leq 1$.

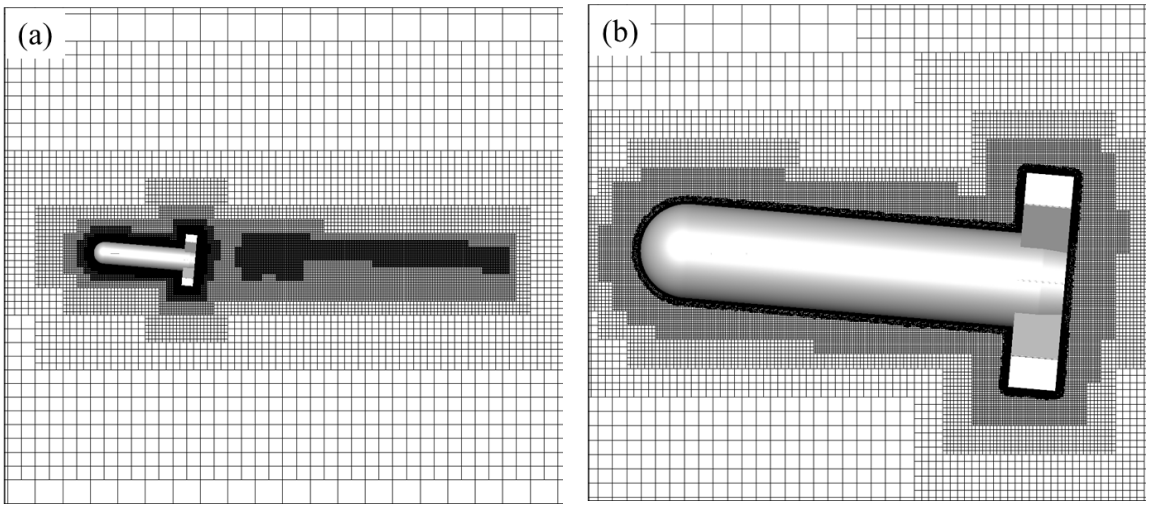

Fig. 2 Computational domain of 8-fin configuration after 3500 iterations using (a) adaptive mesh refinement and (b) zoomed-in view of NB mesh

To validate and compare the computed aerodynamic coefficients, static aerodynamic data were collected through WT experiments. Subsonic experiments at Mach 0.2 were conducted in a continuous flow, in-draft WT with a 0.71-m (28-inch) high by 1-m (40-inch) wide by 2.14-m (84-inch) long test section housed at the DEVCOM Chemical Biological Center at Aberdeen Proving Ground, Maryland. The 40-mm-diameter model was constructed from selective-laser-sintered glass-filled nylon, and the control surfaces were cut from 1-mm-thick spring steel sheet. The model was mounted on a sting with a 0.95-cm (3/8-inch) diameter and 5-degree-of-freedom balance (Modern Machine & Tool Co.). The balance featured ratings of 44.5 N (10 lb) for axial force, 35.6 N (8 lb) for normal force, 22.2 N (5 lb) for side force, and 0.9 N-m (8 inch-lb) for pitching moment and side moment. The blockage ratio for the model (i.e., projected area of projectile divided by the tunnel cross-sectional area) was calculated to be less than 1%, and therefore was assumed to be negligible. Data was obtained in the WT at $-11° \leq \alpha \leq 13°$ in 1° increments, at both 0° and 90° roll orientations. The balance collected 1000 samples after steady-state flow conditions were met at each α. The averaged measured value was computed for each component.

Figure 3 shows a comparison of C_N and C_m resulting from aeroprediction codes and WT experiments. At small α, there is good agreement between all aerodynamic characterization sources. At higher α, there are larger discrepancies, as expected. In general, all computed aerodynamic sources compare reasonably well for normal force coefficient. Furthermore, all aerodynamic sources compare well to experiment. At higher α, the Navier–Stokes CFD results deviate the most from the other aerodynamic sources. The Kestrel Navier–Stokes CFD predicts earlier onset of the decrease in C_N than the other aerodynamic sources. This reduction could be from stall of the canards or the fins. The associated reduction in C_m indicates fin stall is likely contributing to this effect. Canard trailing vortex–fin interaction effects are unlikely at this high of an α, as the vortices usually do not intersect the fins. Missile DATCOM shows a similar effect at nearly the same α but the change in C_m is much less. There are large discrepancies between the aerodynamic sources for C_m. The results suggest that there are discrepancies in the computation of the center of pressure of the vehicle.

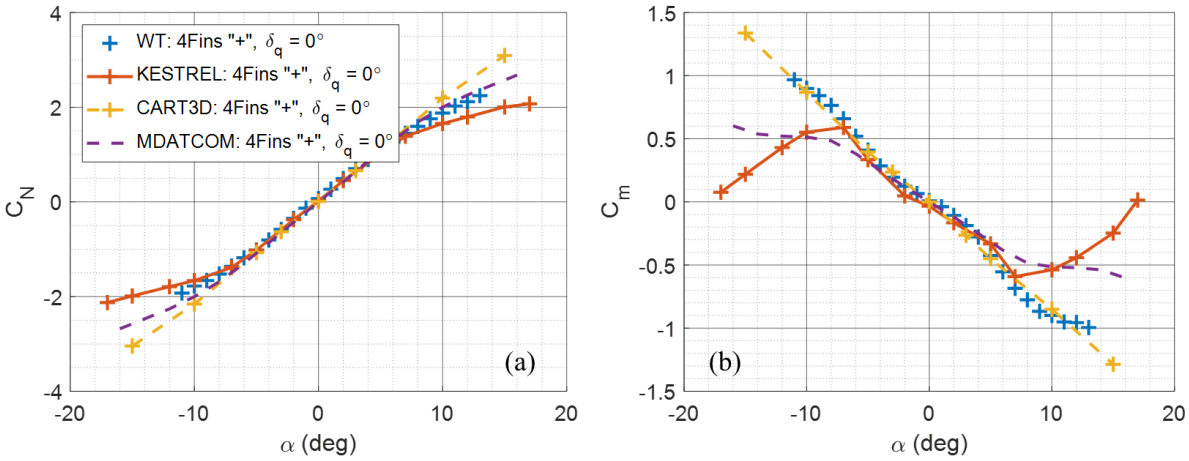

Fig. 3 Distributions of (a) C_N and (b) C_m computed from Missile DATCOM, Cart3D, Kestrel, and measured from WT experiment for zero (δ_q = 0°) pitch deflection at M_∞ = 0.2

Focusing on C_m, we compare DATCOM with Kestrel (KCFD) in Fig. 4. These plots show C_m for all four configurations (two tail configurations and two roll orientations) and two canard deflections (δ_q) at Mach 0.2 and 0.6. For both deflections and at both Mach numbers, we can see the same result we observed in Fig. 3, as Kestrel is predicting an earlier decrease in C_m magnitude compared with DATCOM. However, this effect is most pronounced for the 4-fin configuration in the "+," or $\phi = 0°$ configuration at both Mach numbers, again indicating it is likely due to stall on the horizontal fins, as they are the only fins contributing normal force in this configuration. In the 4-fin x-configuration and both eight-fin configurations, normal force is provided by additional fins, so the reduction in C_N and C_m are less when stall occurs on the fins. Aside from this primary discrepancy, the data is still in good agreement for low and medium α for the remaining configurations.

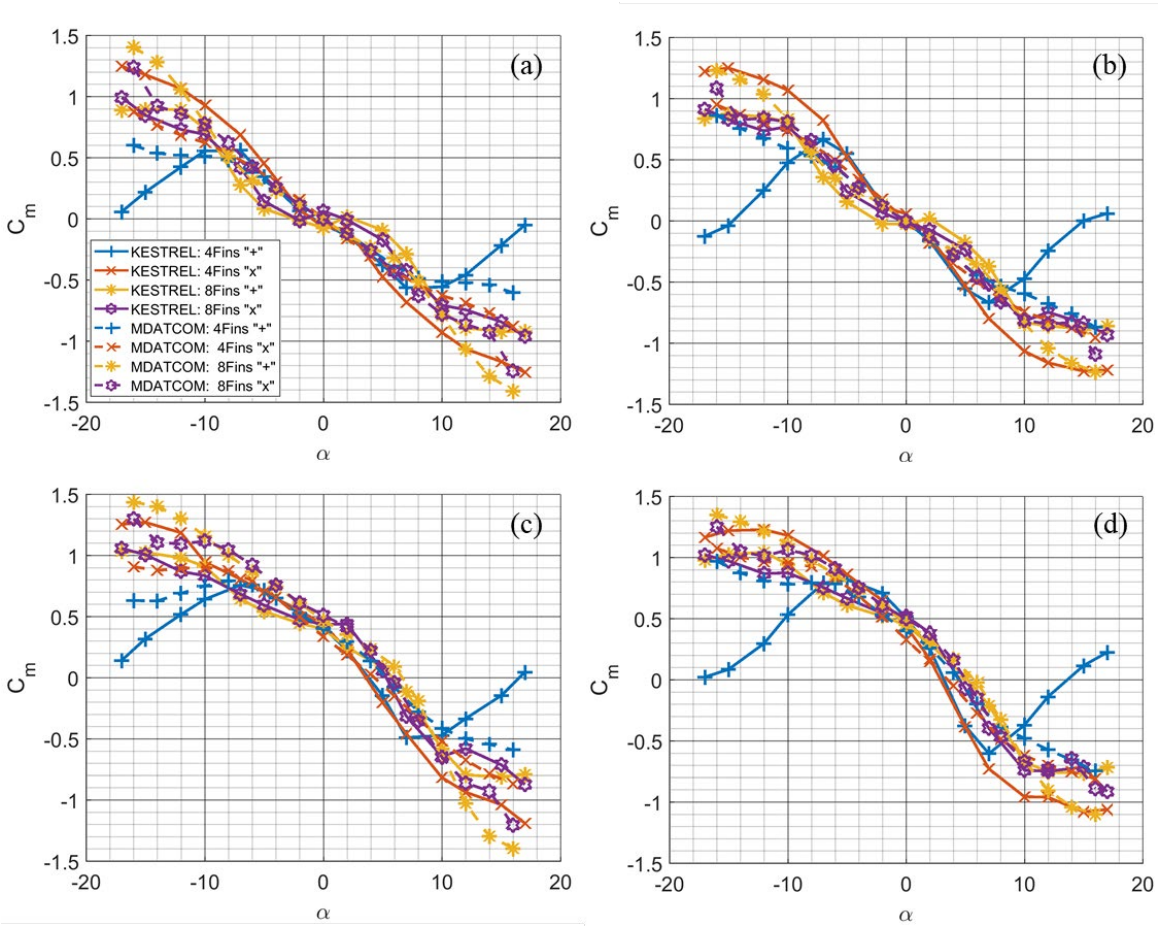

Fig. 4 Distributions of C_m, for all configurations computed from Missile DATCOM (dashed) and Kestrel (solid) for both (a, b) zero ($\delta_q = 0°$) and (c, d) positive pitch deflection ($\delta_q = 5°$) at (a, c) $M_\infty = 0.2$ and (b, d) 0.6

In the case of positive roll maneuver, the canards were deflected ($\delta_p = 5°$) to produce a positive C_l (i.e., clockwise). Figure 5 shows the distributions of C_l for this case at $M_\infty = 0.2$ and 0.6. For both DATCOM and Kestrel results, the total C_l distribution is symmetric with respect to α. Large discrepancies are present between DATCOM and Kestrel results for both 4-fin configurations. The DATCOM results at Mach 0.2 show positive C_l when the canards are deflected for positive roll across the α range investigated. The 4-fin cross "x" configuration results in the largest magnitude of C_l, while the 4-fin "+" configuration shows evidence of adverse roll effects (i.e., reduced C_l) due to canard trailing vortex–fin interactions at low α that reduce the roll effectiveness (e.g., $-6° \leq \alpha \leq 6°$). Increasing α also leads to a reduction in C_l due to leeside shadowing effects and likely vortex–fin interactions. For the 8-fin configurations, the DATCOM results indicate adverse roll effects are significant for both 8-fin configurations. The fins in this configuration have less span, occupy twice the circumferential distribution around the projectile body, and appear more susceptible to vortex–fin interactions. The Kestrel results for the 4-fin

configurations indicate adverse roll effects from vortex–fin interactions across the α range investigated with significant reduction in roll moment even at low α. The Kestrel and DATCOM results compare better for the 8-fin configuration, with both also showing significant adverse roll effects independent of α. Both codes predict roll reversal above 13°–14°. Similar trends are shown for Mach 0.6, where Kestrel now predicts roll reversal below 10° for all configurations. In addition to magnitude, the nonlinear behavior in the distribution of C_l for each given 8-fin variant compares well to the respective computed distributions from Kestrel. The 8-fin cross "x" variant seem to produce a constant total C_l value across α, whereas the 8-fin plus "+" variant produces a nonlinear distribution exhibiting a maximum value at α = 0°, and a minimum value at approximately α = ±7°.

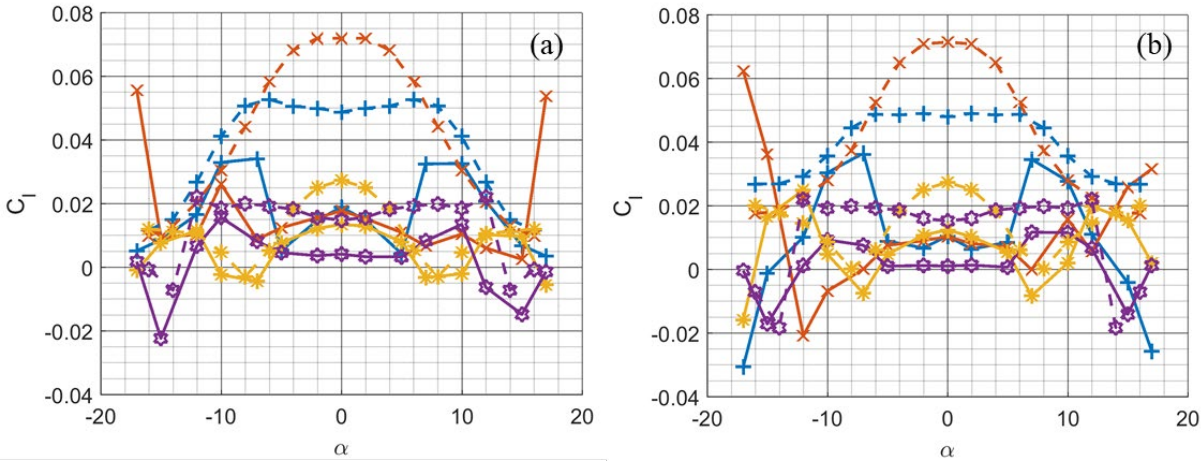

Fig. 5 Distributions of C_l for all configurations computed from Missile DATCOM (dashed) and Kestrel (solid) for positive roll deflection ($\delta_p = 5°$) at (a) M_∞ = 0.2 and (b) 0.6 (same legend from Fig. 4)

Both aeroprediction codes predict the longitudinal aerodynamic coefficients reasonably well, especially in the range $-10° \leq \alpha \leq 10°$. The vortex models in Missile DATCOM predict the effects of vortex-fin interaction. Kestrel did not match the trend in C_m for the WT data in the 4-fin configuration at the higher angles of attack. While the compressible flow numerical solver in Kestrel has performed well at this Mach number, an incompressible solver is now also available. A comparison of the prediction from the incompressible solver would be informative but was not performed due to time constraints. DATCOM prediction of roll moment in the 4-fin configuration did not compare as well to the Navier–Stokes prediction, which predicted significantly more-adverse roll-interference effects from canard vortex–fin interference. Predictions of adverse roll-moment effects in the 8-fin configuration compared much better, both in magnitude and general trends, with angle of attack. Both aeroprediction codes also predict roll reversal ($C_l < 0$) at similar angles of attack.

3.2 NASA Strake-Tail Missile

NASA Langley Research Center investigated several body build-up configurations for a tail-controlled strake missile in a WT campaign.[19] Figure 6 shows the seven configurations tested. Only Configuration 1 (body-tail-long strake) is considered in the present study. Missile DATCOM, Cart3D (flowCart), and Kestrel (KCFD) simulations were completed for the configuration and flow conditions reported in a similar study by Rosema et al.[20]

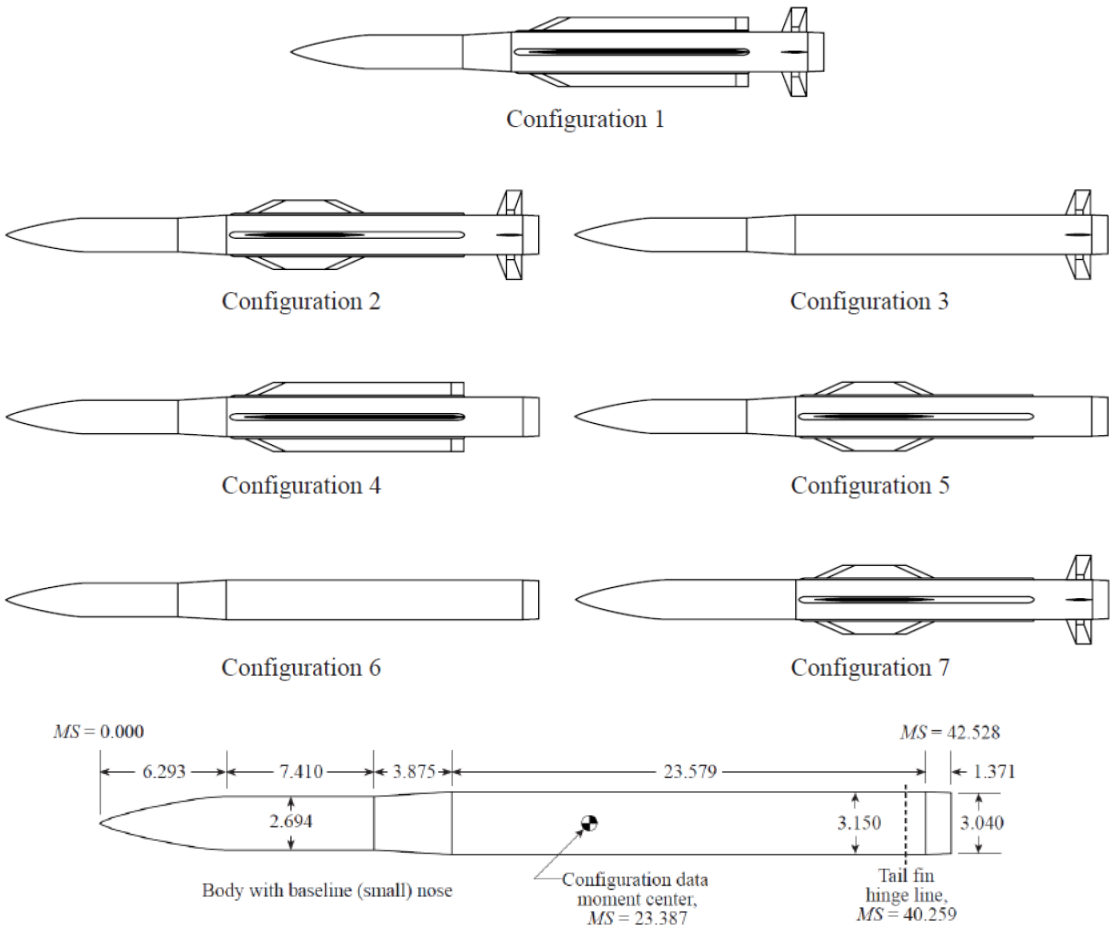

Fig. 6 Missile configurations from Allen[19] and dimension of body

Figure 7 shows the Cart3D Cartesian mesh for Configuration 1 (long strake) in two roll orientations, $\phi = 0°$ and $\phi = 45°$. The cut-plane is through the vertical (pitch) plane. It was recently shown by Doyle et al.[21] that improved predictions are obtained using a beta version of DATCOM in which the vorticity is distributed along the strake tip. Doyle et al.[21] used Configuration 1 to study the comparison of various methods. In this section, we highlight some of the author's contributions to that paper.

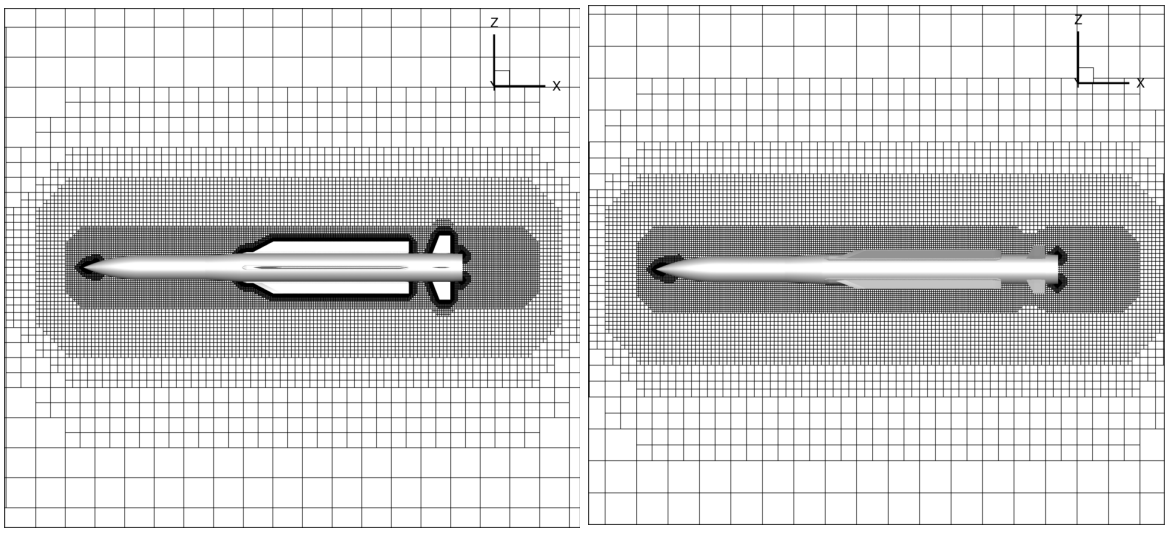

Fig. 7 Cart3D mesh for Configuration 1: ϕ = 0° (left) and ϕ = 45° (right)

Figure 8 compares the pitching moment in the non-rolled plane, $C_{m_{NR}}$, for two roll configurations, $\phi = 0°$ and $\phi = 45°$, and four different Mach numbers between 0.6 and 3.95. We notice immediately that the beta version of DATCOM performed better than the original in predicting $C_{m_{NR}}$, providing a better prediction of the missile stability than the standard version. At $\phi = 0°$, Cart3D shows good agreement with Kestrel predictions at low to medium α, but Cart3D overpredicts the pitching moment magnitude above $\alpha = 15°$ for Mach 0.6 and 1.70. Cart3D and Kestrel compare well for the higher Mach numbers. Both Cart3d and Kestrel compare well with the WT data, especially at the higher Mach numbers.

In the $\phi = 45°$ roll configuration (right side of Fig. 8), the pitching moment profile shows more changes in slope due to the additional vortical flow structures that shed from the strakes that are now in the "x" orientation with respect to the freestream flow. At Mach 0.6, Cart3D and Kestrel $C_{m_{NR}}$ predictions compare well to the WT data up to $\alpha = 4°$, then Cart3D overpredicts the magnitude while Kestrel underpredicts the magnitude at higher angles. Kestrel predicts the general shape of the profile including the decrease in pitching moment magnitude near $\alpha = 16°$. At Mach 1.7, both Cart3D and Kestrel predict this decrease in pitching moment magnitude, now approximately $\alpha = 14°$. Cart3D predictions improve with increasing Mach number, matching Kestrel at Mach 3.95. As expected, Kestrel provides the most-accurate predictions overall. In this roll orientation, the accuracy of Missile DATCOM predictions of $C_{m_{NR}}$ varies with Mach number and α.

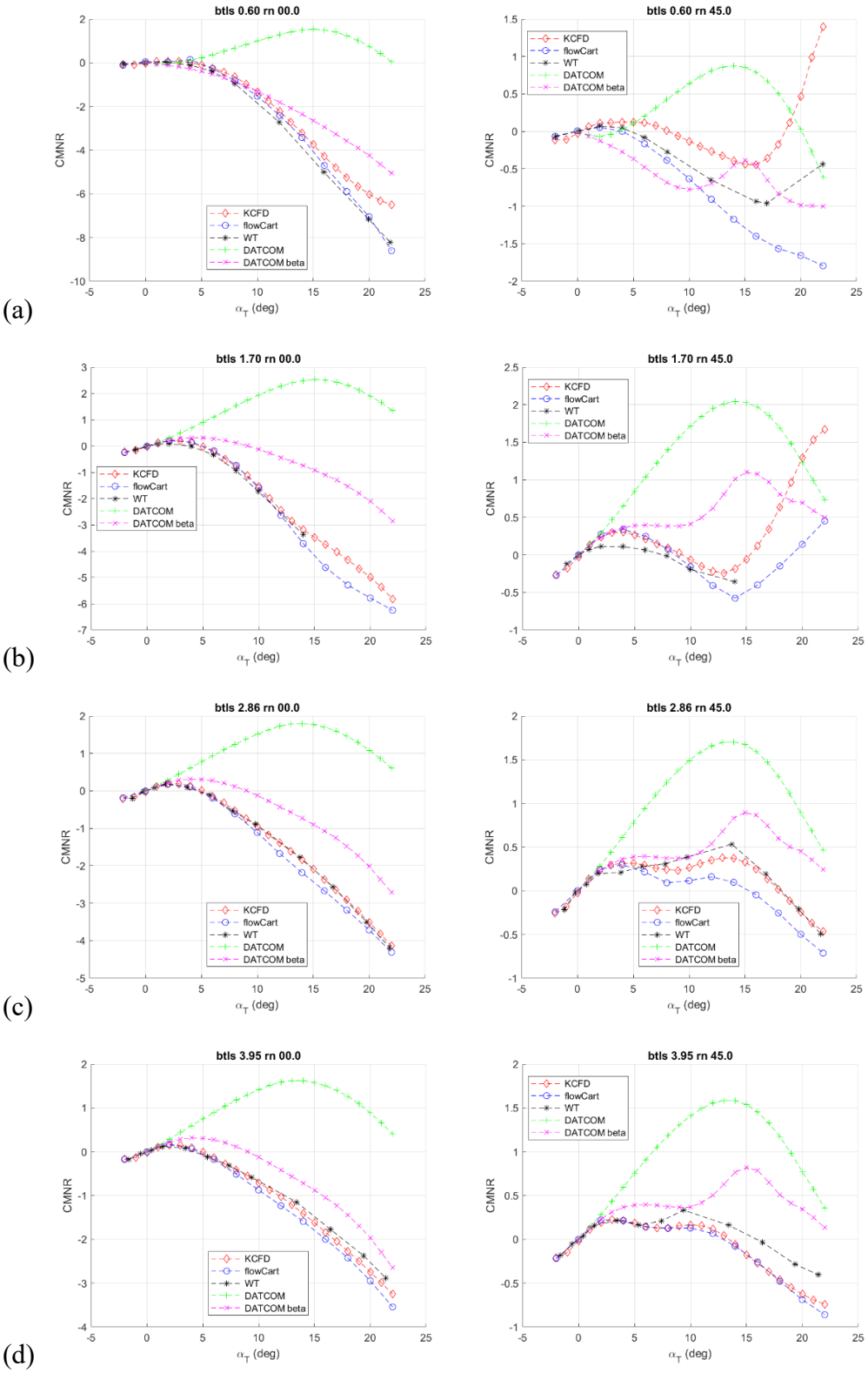

Fig. 8 $C_{m_{NR}}$ **variation with** α_T **from WT and aeroprediction codes for Configuration 1 at (left)** ϕ **= 0° and (right)** ϕ **= 45° (right): (a) Mach 0.6, (b) Mach 1.7, (c) Mach 2.86, and (d) Mach 3.95**

Figure 9 shows results for the normal force in the nonrolled plane, $C_{N_{NR}}$, at Mach 1.18 at four roll angles. Cart3D and Kestrel predictions compare well with the WT data with some noticeable overprediction above $\alpha_T > 10°$ and $\phi = 33°, 57°$, which are near the "x" roll orientation. In these roll orientations, DATCOM provides better normal force predictions than those angles closer to the "+" roll orientation ($\phi = 12°, 78°$). Figure 10 (from Doyle et al.[21]) shows the ϕ-sweeps of normal force at Mach 1.18 at four angles of attack. These plots were extracted from α-sweep data generated from the aeroprediction codes and WT data. Note that the scale on these plots magnifies the differences among the data at the equivalent data points in Fig. 9. Cart3D provides nearly the same normal force prediction as the Navier–Stokes solver Kestrel (and Raven CFD and OVERFLOW, described in Rosema et al.[20]), indicating viscous effects do not dominate the flow physics. These codes overpredict normal force by 5%–10% but accurately match the trend with roll orientation. The experimental version of DATCOM provides a much better prediction of roll moment but still underpredicts the normal force by a significant amount. The trends of pitching moment were similar, with Cart3D becoming less accurate at the higher angles of attack, as presented in Fig. 8. The difference in pitching moment from the aeroprediction codes and WT experiments were larger, but this was exaggerated due to the center or pressure being close to the center of gravity, the moment reference point. The prediction of center of pressure ($x_{cp} = -C_{m_{NR}}/C_{N_{NR}}$) showed that the differences equated to only 0.2 cal even at the higher α.[21]

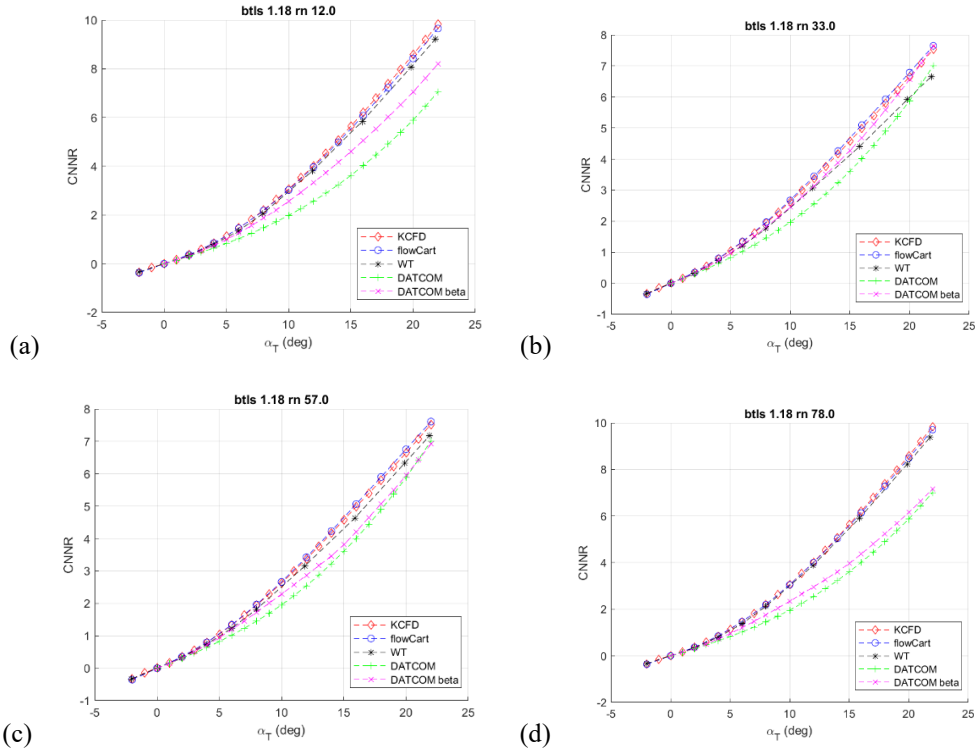

Fig. 9 $C_{N_{NR}}$ variation with α_T from WT and aeroprediction codes for Configuration 1 at Mach 1.18 and ϕ = (a) 12°, (b) 33°, (c) 57°, and (d) 78°

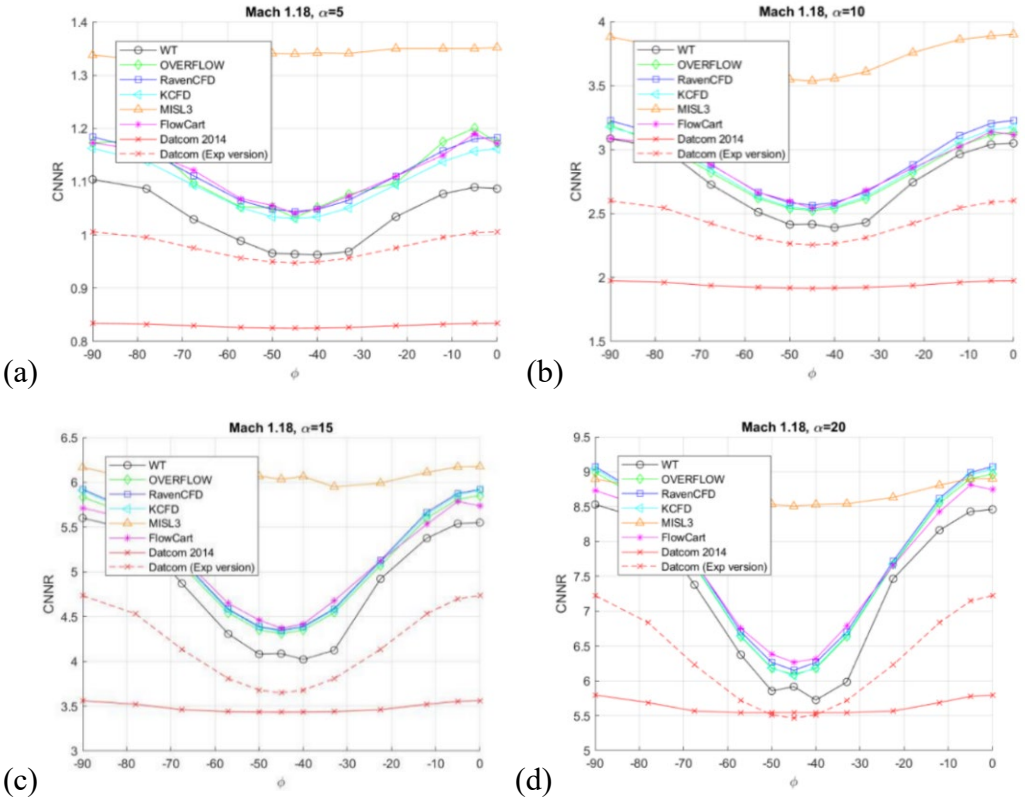

Fig. 10 $C_{N_{NR}}$ variation with roll angle from WT and aeroprediction codes for Configuration 1 at Mach 1.18 and α = (a) 5°, (b) 10°, (c) 15°, and (d) 20°

The Kestrel RANS predictions showed good agreement with the WT data for Configuration 1 forces and moments. Predictions of the individual fin loads and fin centers of pressure, not shown here, were also good.[21] These RANS predictions captured all the complex vortex interactions required to predict the aerodynamic coefficients in a multi-finset configuration up to moderate angles of attack using a production-level mesh of 35 million cells.[21] Cart3D predictions closely matched the WT data and RANS predictions for a large part of the simulation matrix, with deficiencies usually above $\alpha_T = 15°$. This is excellent performance for an intermediate-level missile aerodynamic database when complex vortex-dominated flow is present. Missile DATCOM 2014 has known deficiencies in modeling missiles with long strakes due to all the vorticity being shed from the trailing edge of the strake. An experimental version of Missile DATCOM, distributing the shed vorticity chordwise along the strake tip, provided improved predictions.[21] While the RANS predictions performed well for this missile configuration, including those due to asymmetric orientations, there are examples of cases where production-level CFD methods fall short for some configurations (e.g., missile roll angle, angle of attack, Mach number). Proper care must be used to identify those

configurations where small errors in vortex trajectory and strength might lead to large errors in loads—especially in the rolling moment.

3.3 Air Force Finner Missile

The AFF has a diameter of 30 mm (1 cal) with a 2.5-cal tangent ogive followed by a 7.5-cal cylindrical body. The AFF has four clipped-delta fins with a 1.333-cal root chord, a 0.67-cal tip chord, and a semi-span of 0.5 cal. There was a 0.25-cal bevel on the leading and trailing edges of the fins. The center of gravity was located 4.8 cal from the nose tip. A schematic of the AFF is shown in Fig. 11. The AFF has been used as a reference missile for many years and has been extensively tested in aeroballistic, free-flight ranges, and WTs, and is the subject of several numerical investigations.[22–27]

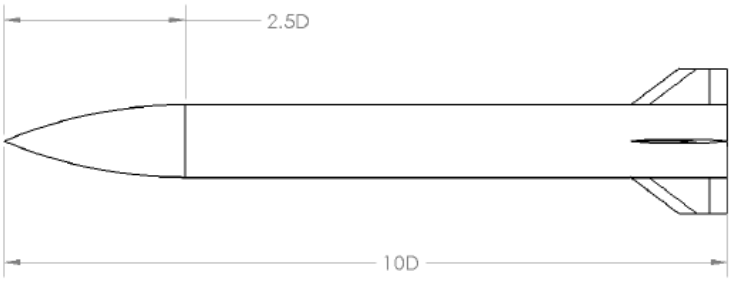

Fig. 11 AFF Missile (1 cal = 0.03 m)

Aerodynamic predictions were computed using Missile DATCOM, Cart3D, and Kestrel and were compared with experimental data. Figure 12 shows the Cartesian mesh with pre-specified refinement regions used in Cart3D simulations. Most Cart3D simulations were performed with this type mesh, but the effect on the prediction accuracy of using the adjoint adaptive mesh refinement method was also investigated. Figure 13 shows the unstructured mesh used in the Kestrel simulations. This mesh predominantly consists of tetrahedral cells with layers of prismatic cells projected off the solid wall boundaries to capture the boundary layer.

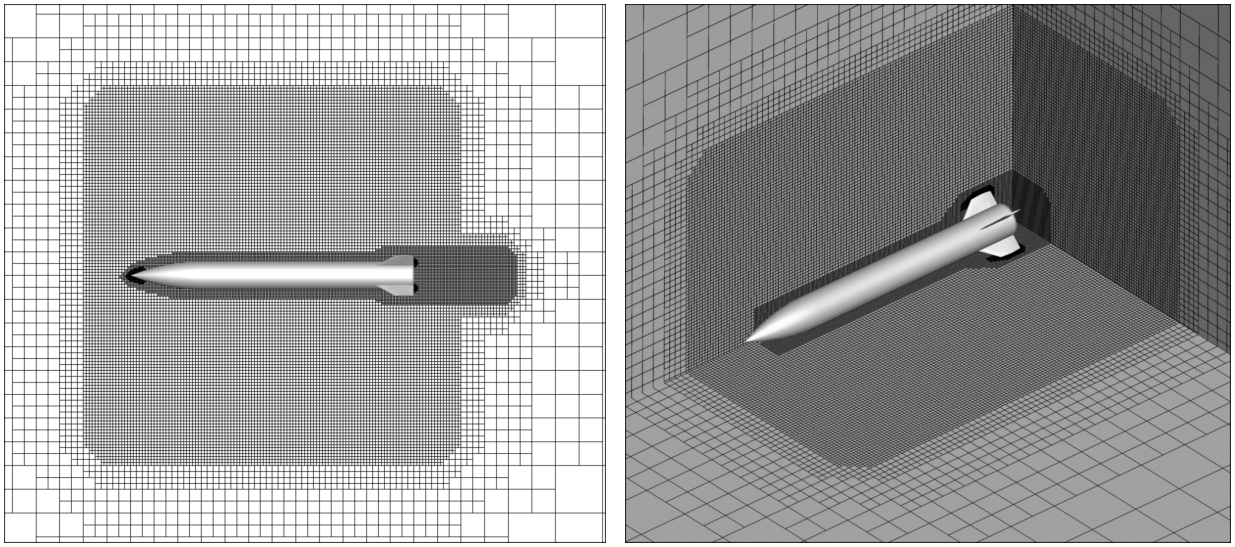

Fig. 12 Cart3D mesh generated for the standard AFF configuration

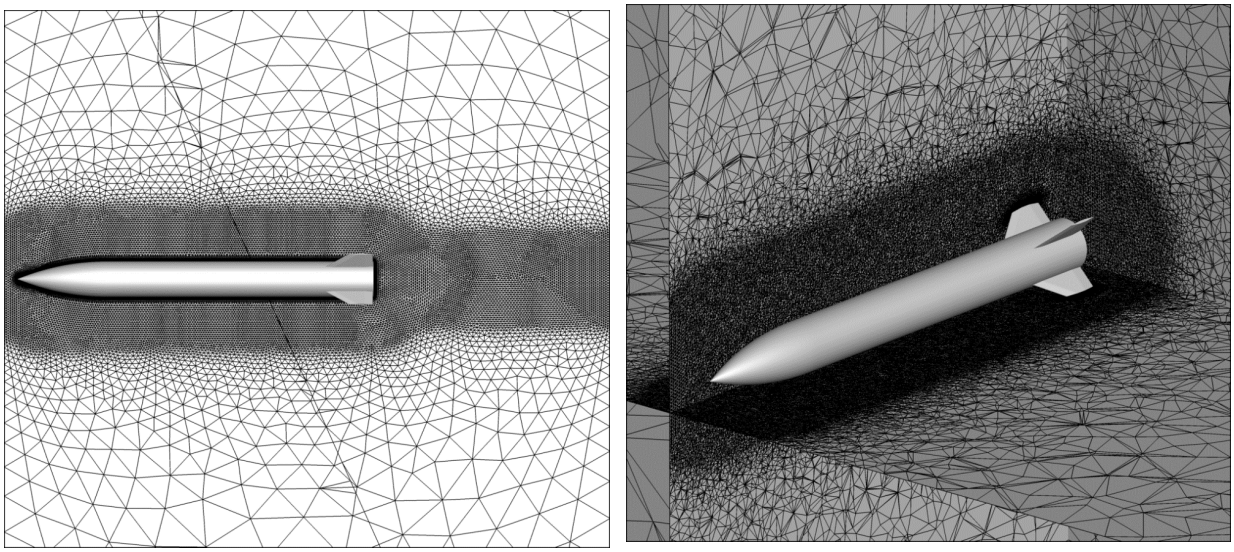

Fig. 13 Capstone mesh generated for the standard AFF configuration for Kestrel simulations

Because the standard AFF is a typical ogive-body-fin-configuration missile, it was expected that all three aeroprediction methods would adequately predict the aerodynamic properties. Limitations of the models in the semi-empirical DATCOM or the inviscid nature of Cart3D tend to be observed as angle of attack increases. Figure 14 shows the drag and normal force at Mach 2.0, 2.5, and 3.0 compared with experimental data. The experimental data was obtained from aeroballistic spark range free-flight experiments at Mach 2.0 and 2.5 via single-fit aerodynamic

derivative coefficients. The prediction of C_D is good for all three prediction methods. DATCOM overpredicts the drag until $\alpha > 20°$. At all three Mach numbers, Cart3D underpredicts the drag at lower angles of attack—as expected due to the lack of viscous drag component—but is still close to the Kestrel prediction. The Cart3D drag prediction approaches the viscous Kestrel prediction as α increases and the pressure component of the normal force dominates the drag. The prediction of normal force by Cart3D agrees well with Kestrel predictions at all three Mach numbers. Both compare well with experimental data at Mach 2.0 but overpredict the experimental data above $\alpha \geq 4°$ at Mach 2.5. The experimental data was calculated versus α using the normal force derivative values, and a nonlinear term was not available. Additionally, the experimental data used to calculate C_N was extrapolated to Mach 2.5 from 2.42, but this should have minimal effect. DATCOM predicts normal force well up to about $\alpha = 6°$, then slightly overpredicts the value.

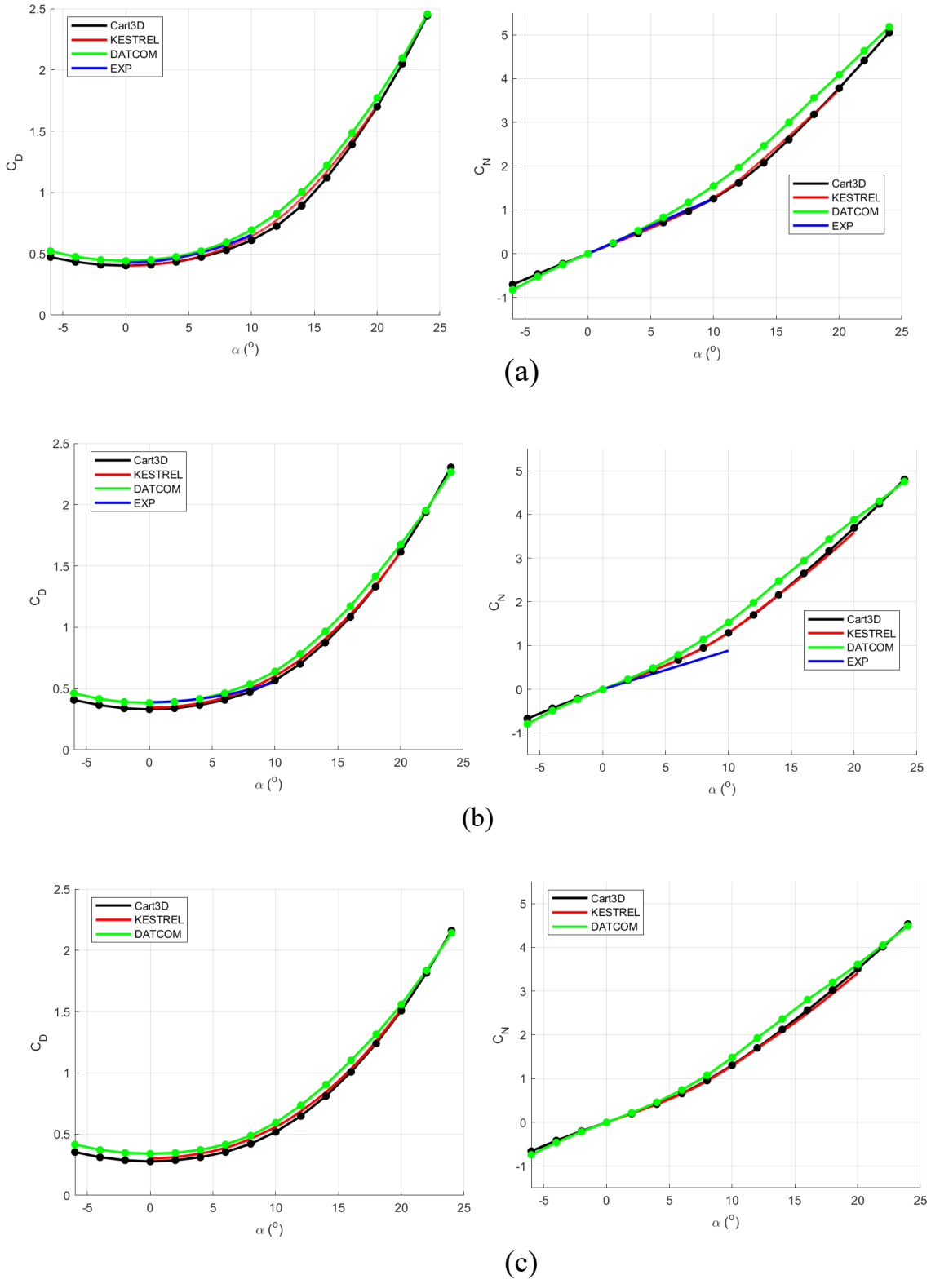

Fig. 14 C_D (left) and C_N (right) at Mach (a) 2.0, (b) 2.5, and (c) 3.0 for the standard AFF configuration

In the prediction of pitching moment, all the codes were similar up to $\alpha = 5°$ at all three Mach numbers, with DATCOM predicting a slightly steeper slope (more stability). DATCOM also predicts little or no nonlinearity, even up to $\alpha = 24°$. Both Cart3D and Kestrel predicts a nonlinear increase in C_m magnitude that starts between $\alpha = 5°$ and 10°, depending on Mach number. Cart3D tends to overpredict the magnitude of C_m by a small amount in the nonlinear region compared with Kestrel. The pitching moment profile predicted by Kestrel shows some undulations at Mach 2.0 and 2.5, especially at $\alpha = 12°$ and Mach 2.0. The Kestrel data was produced as quasi-steady sweeps at low reduced frequency—similar to a WT sweep—where data is available at every time step and provide a higher resolution profile. This data was compared with single steady runs at $\alpha = 8°$ and 16° and the results compared well. These results are shown in Fig. 15.

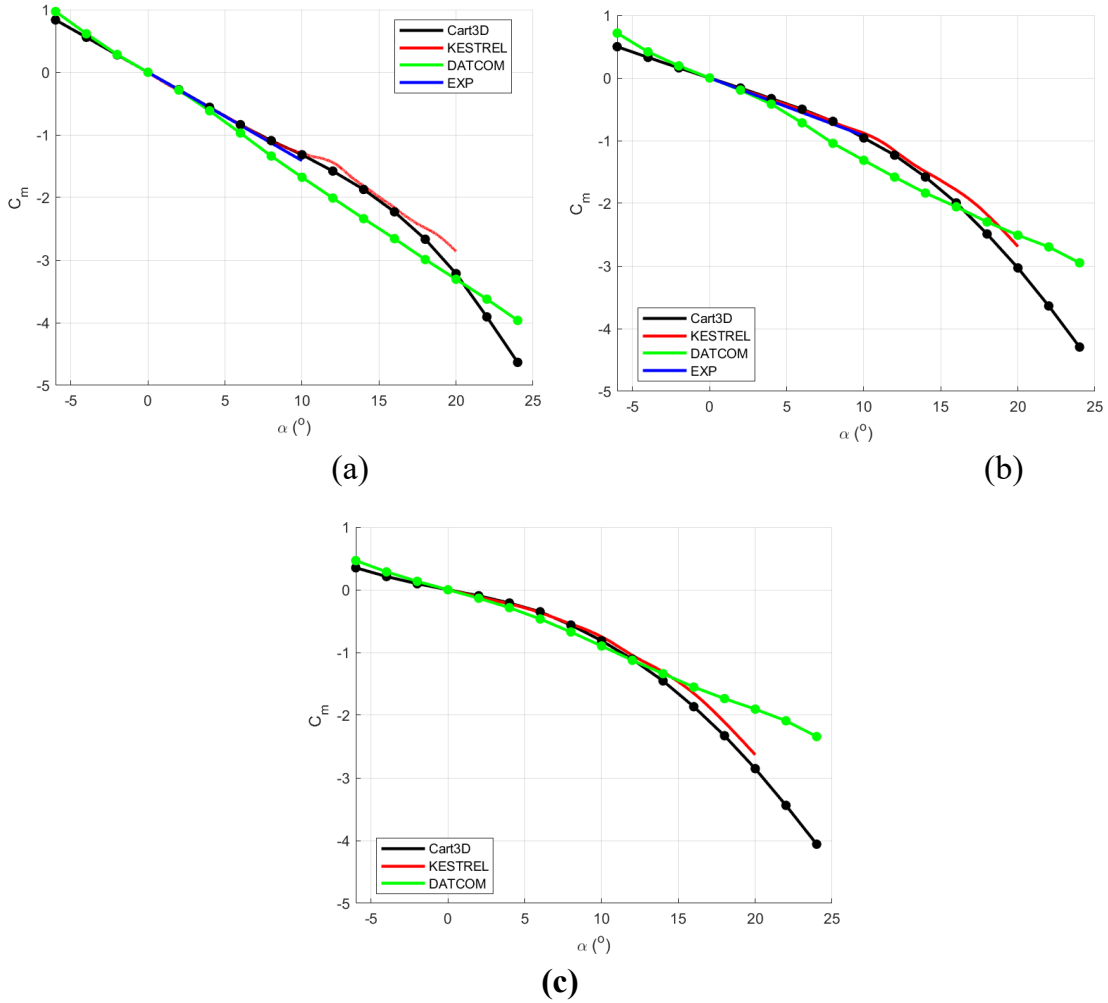

Fig. 15 C_m at Mach (a) 2.0, (b) 2.5, and (c) 3.0 for the standard AFF configuration

The nonlinear variation in pitching moment is likely due to the symmetric body vortices that form at the ogive region, usually starting at about $\alpha = 10°$. These vortices grow in size and intensity as α increases and change the normal force distribution along the body. In this case, the increase in the normal force at the higher angles (Fig. 14) is distributed farther rearward, thus moving the center of pressure rearward and leading to the increased C_m. Above about $\alpha = 20°$, the vortices become asymmetric and lead to larger side force and yaw moments in addition to further effects on the normal force and pitching moment.[28] This is likely the reason for the steepening of the C_m profile we see at higher α. DATCOM has vortex models to predict these effects, and it picked up the trends due to this effect in the subsonic results of Section IV.A. However, it did not predict this effect in the supersonic Mach regime.

Some further insight into the discrepancies in C_m predictions can be found in the pressure distribution on the AFF body surface along the symmetry plane (Fig. 16). In this case, at $\alpha = 12°$, all three codes predict the pressure distribution over the front half of the missile fairly similarly, particularly on the windward side (upper profiles) of the missile. On the latter half of the body, DATCOM shows neither the difference in pressure (no body lift), nor the effect of the fins. Kestrel shows lower predicted pressures on the suction side (lower profiles) than Cart3D, which produces more body lift. Increased body lift aft of the center of gravity location (x = 0.14) is stabilizing; however, the differences in the C_p prediction in the tail region ($x \geq 0.27$) lead to Kestrel predicting slightly less stability (Fig. 16). The differences in the C_p profiles in the tail region are the result of the difference in the predicted vortex structure in the inviscid versus viscous simulation. Further study will include comparing the qualitative nature of the leeside vortices among the prediction codes.

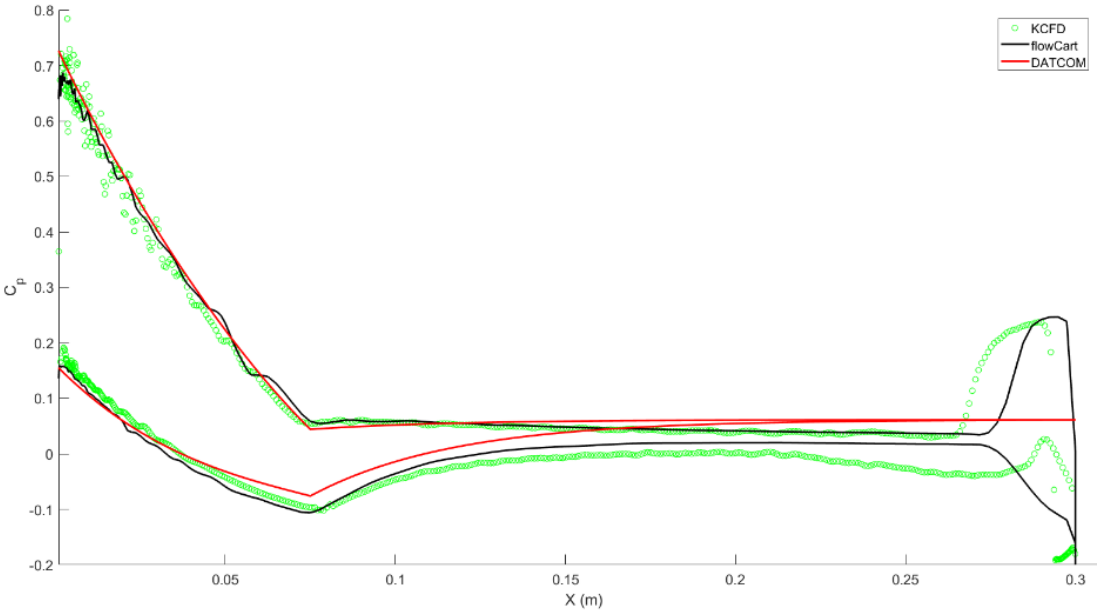

Fig. 16 C_p distribution on the AFF body surface in the symmetry plane for Cart3D, Kestrel, and DATCOM at Mach 2.0 and $\alpha = 12°$ for the standard AFF configuration

All three prediction methods performed reasonably well for this standard ogive-body-fin configuration. DATCOM did not predict the nonlinear trend in pitching moment, which are believed to be due leeside vortex formation at the moderate and high angles of attack. The small differences in pitching moment prediction at the higher angles attack between Cart3D and Kestrel are also likely due to the lack of viscous effects near the missile body not modeled in Cart3D.

3.4 Laboratory Technology Vehicle

ARL is currently testing a generic gun-launched projectile to investigate the aerodynamics, control, and navigation technologies related to high-speed, long-range artillery.[29] An aerodynamic design optimization was used to determine the shape of this LTV.[30] Figure 17 shows a schematic of the LTV. The nose tip was modeled as a blunt nose defined by a bluntness radius that is 0.1 of the diameter (i.e., 0.1 cal). The Von Karman ogive nose shape was used, with the length of the ogive section defined to be 0.3 of the overall length (OAL) of the projectile. The center of gravity of the flight vehicle was defined to be 0.6 of the OAL of the projectile. The body section was modeled as a cylinder. Additionally, the aft section included a 7°, 0.5-cal boattail. The projectile was designed to be sabot-launched from an 8-inch-diameter gun with no deploying aerodynamic surfaces. A leading-edge sweep angle of 83° was used. All control surfaces had a root thickness of 4 mm and tapered down to 2 mm at the tip. The design parameters of the projectile are summarized in Table 1.

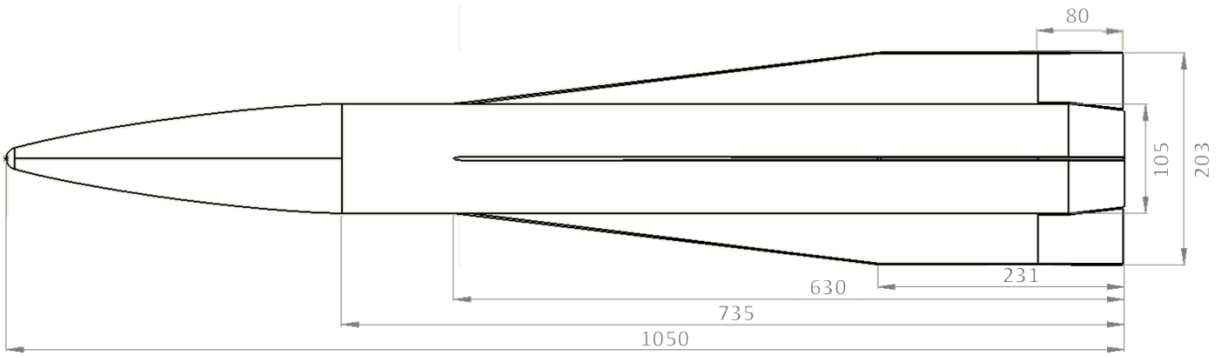

Fig. 17 Schematic of LTV (dimensions given in millimeters)

Table 1 LTV parameters

Vehicle configuration	Diameter (mm)	Length-to-diameter	Ogive length of OAL	No. of fins	Root fin chord (cal)	Tip fin chord (cal)	Fin span (cal)
Body fin	105	10	0.3	4	6	2.2	1.935

The LTV was evaluated using Missile DATCOM, Cart3D, and CFD^{++}. The meshes used for Cart3D and CFD^{++} are shown in Figs. 18 and 19, respectively. The Cart3D simulations were completed using AMR to efficiently acquire the most accurate inviscid solutions for each simulation. Mesh density regions were implemented on the Cart3D meshes to refine the mesh near the surface as well as in the wake region to help resolve flow structures. These regions in the Cart3D meshes are further refined during the flow solution via the AMR. The adjoint mesh adaption techniques available in Cart3D were not used in this study. The computational domain of the Cart3D meshes consisted of approximately 10 million Cartesian cells and extended approximately 14 projectile lengths from the center of the projectile. The mesh used for the CFD^{++} simulations was generated using Capstone (version 9.1)[17] mesh generator. The total mesh size was approximately 43 million cells, consisting of triangular surface cells, with prism layers used along the surface, and tetrahedral cells for the rest of the domain. The computational domain extended approximately 20 projectile lengths in all directions from the center of the projectile. The average cell size of the cylindrical density box (i.e., 2 cal in radius, spanning 1 cal forward to 5 cal back of the projectile) was approximately 0.002 m. The first cell wall spacing of the prism layers were set to 3×10^{-7} m to ensure $y^+ \leq 1$ along the surface of the projectile for all Mach numbers of interest.

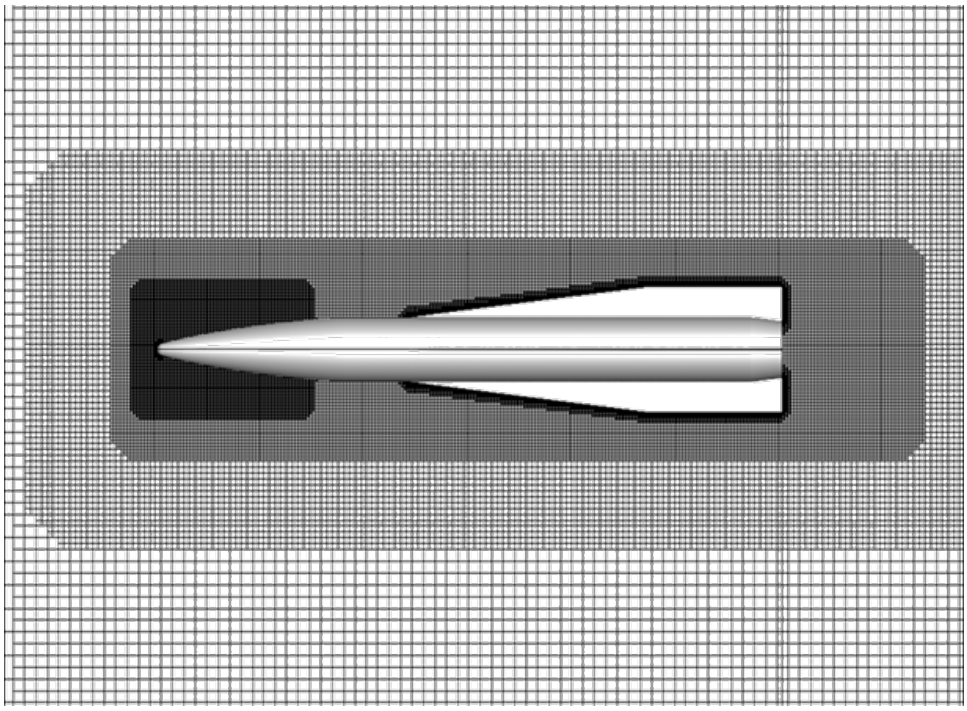

Fig. 18 Computational domain used for Cart3D

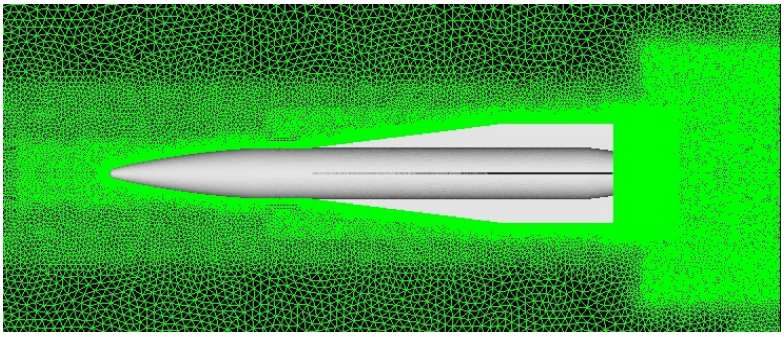

Fig. 19 Computational domain used for CFD^{++}

Figures 20 and 21 show the comparison of DATCOM, Cart3D, and CFD^{++} predictions of the LTV aerodynamics in the "+" orientation ($\phi = 0°$) and the "x" orientation ($\phi = 45°$). The aerodynamic coefficients computed by DATCOM are presented as solid lines; the coefficients computed by Cart3D are presented as open triangle symbols; and the coefficients computed by CFD^{++} are presented by open circle symbols. The DATCOM dataset underpredicts the C_A of the vehicle compared with the CFD^{++} data (Fig. 20a). However, the C_A trend across Mach number compares relatively well. Overall, all aerodynamic sources show good agreement for C_N (Fig. 20b). The results suggest that DATCOM code is suitable to accurately predict the C_N for low-aspect-ratio finned projectiles at low and

moderate α. At higher α, the values deviate, suggesting that high α nonlinear flow physics are present and are not well predicted in the semi-empirical code.

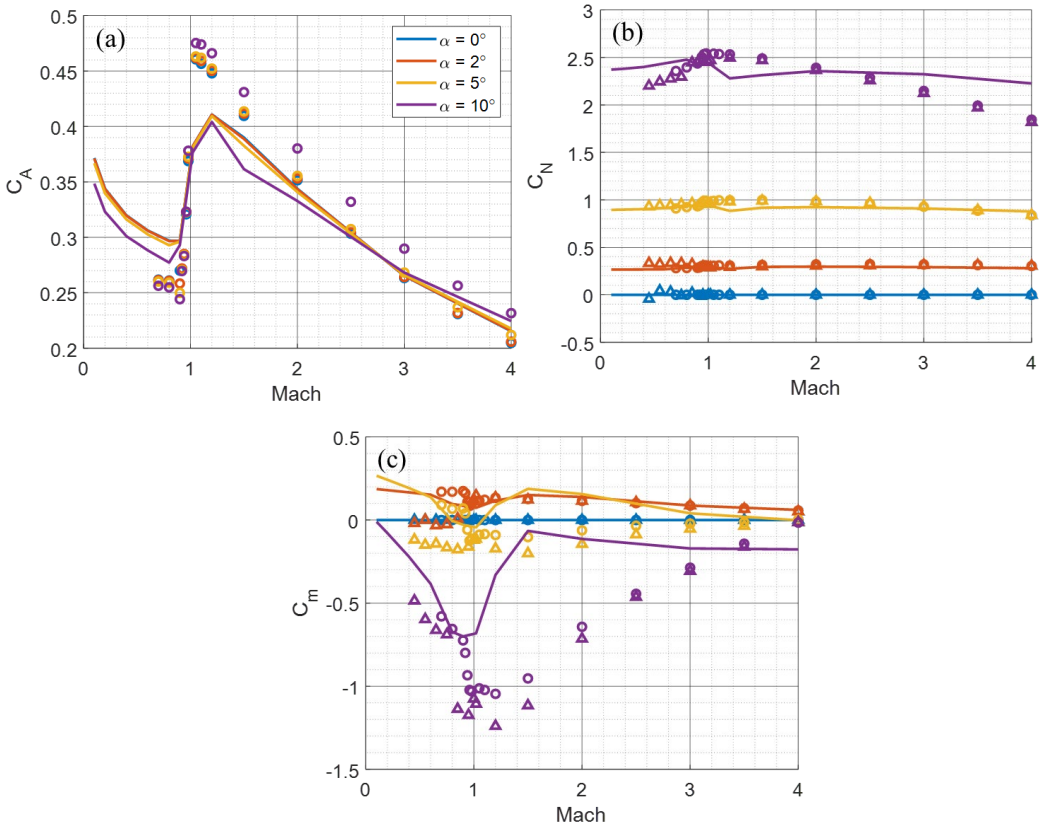

Fig. 20 Computed (a) C_A, (b) C_N, and (c) C_m coefficients of the entire vehicle, computed by DATCOM (solid lines), Cart3D (open triangle symbols), and CFD^{++} (open circle symbols) at $\phi = 0°$

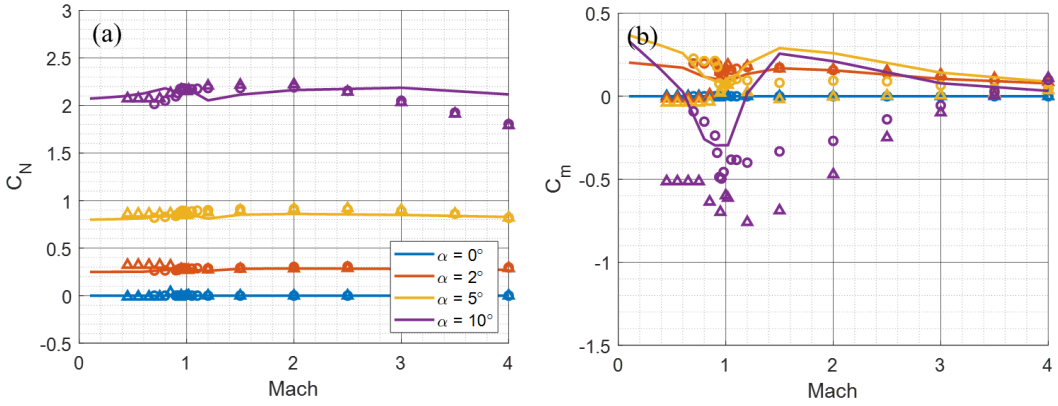

Fig. 21 Computed (a) C_N and (b) C_m coefficients of the entire vehicle, computed by DATCOM (solid lines), Cart3D (open triangle symbols), and CFD^{++} (open circle symbols) at $\phi = 45°$

The largest discrepancies are observed for the predicted C_m (Fig. 20c). The main contributor to this effect is the difference in the predicted location of the center of pressure between DATCOM and the CFD codes. Although the C_N was accurately predicted, the center of pressure location, and therefore C_m was not predicted well. Overall, the CFD results show larger values of C_m, specifically at higher α. The results suggest that DATCOM may provide a more conservative (i.e. center of pressure location predicted further forward, therefore reduced stability) result when determining the static stability of low aspect ratio finned projectiles. At the aerodynamic $\phi = 0°$ angle in Fig. 20, Cart3D and CFD^{++} compare reasonably well. The largest discrepancies are present in C_m at subsonic and low supersonic speeds (Fig. 20c). At higher Mach numbers, the Reynolds number is high, where viscous effects become less significant.

The C_N and C_m distributions of the entire vehicle at $\phi = 45°$, are presented in Fig. 21a and b, respectively. At this orientation, the leeward fins are in the wake of the body and at a lower Mach number than the windward fins. The exposed windward fins are more effective than the leeward fins, which causes the center of pressure to move forward. This is shown in the significant reduction in C_m at the same flight conditions (Fig. 21b). The results show an approximate reduction of 40% in C_m compared with the ϕ = 0° orientation. This finding is important for projectile designers because the static C_m is used to evaluate a vehicle's static stability. The most noteworthy discovery is the large discrepancies of computed C_m between the CFD predictions (Fig. 21b). DATCOM was unable to accurately predict the C_m at the higher α. The Cart3D results show a significant overprediction (approximately 40%) of the C_m magnitude compared with CFD^{++} at higher α across Mach number. The results suggest that viscous effects, specifically the viscous rollup of vortical structures, play an important part in the computed C_m.

To better visualize the discrepancies between Cart3D and CFD^{++}, the generation and advection of the vortical structures produced by the fins were studied. Qualitative plots of scaled Q-criterion iso-surfaces superimposed with contours of pressure coefficient on the surface of the flight body projectile at $\alpha = 10°$ and $M_\infty = 2$, computed from Cart3D and CFD^{++} at $\phi = 45°$, are presented in Fig. 22. The scaled Q-criterion iso-surfaces allow for visual observation of the vortical structures formed at the tip of the fins. The iso-surface value was set to 1.5 and colored based on the magnitude of streamwise vorticity at the same location. The surface-pressure coefficient contour levels were set to be continuous between –0.2 and 0.2. The computed vortical flow structures predicted by Cart3D and CFD^{++} are in relatively good agreement. There are some discrepancies as the aerodynamic roll angle increases. This is natural, since the inviscid code does not include the viscous roll-up as the vortex is formed along the fin tip. This effect can be observed in

Fig. 22, where the roll-up in the Cart3D solutions begin at the fin tip, while the roll-up in the viscous CFD^{++} solutions are delayed and occur slightly inboard of the tip. Additionally, the primary difference is the presence of a vortex structure near the root of the windward side of the leeward fin. Cart3D is unable to resolve the vortical flow structure along the root on the windward face of the leeward fins. These root vortices are predominantly a viscous effect; therefore, Cart3D will never be able to resolve these small structures. These relatively small discrepancies in the structure and location of vortices ultimately result in noticeable discrepancies in the computed aerodynamic coefficients of the projectile.

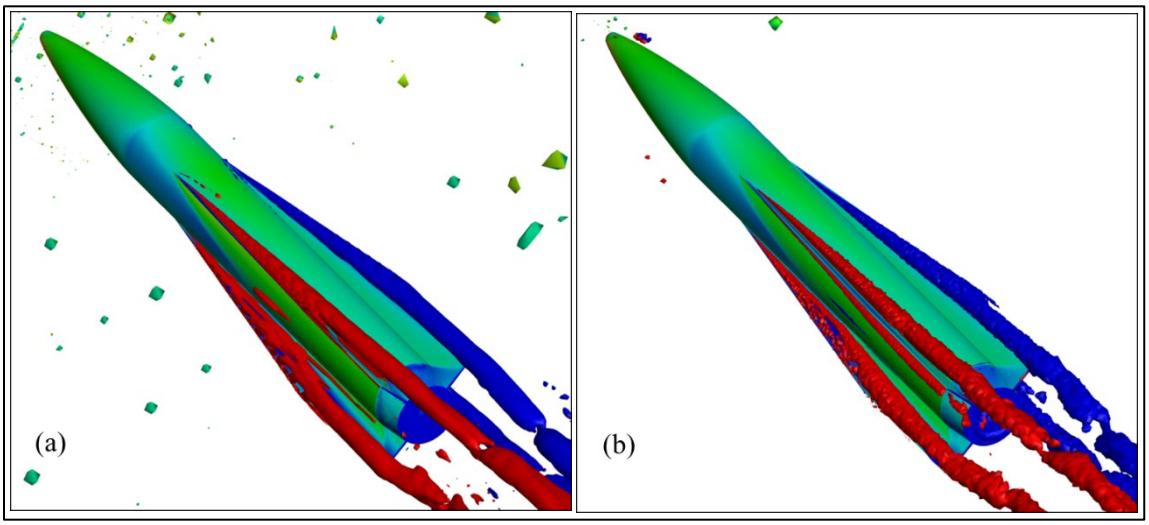

Fig. 22 Surface contours of pressure coefficient superimposed with iso-surfaces of scaled Q-criterion (Qs = 1.5) colored by streamwise vorticity at $\phi = 45°$ and computed by (a) Cart3D and (b) CFD^{++}

A comprehensive effort was undertaken to aerodynamically characterize a low-aspect-ratio finned projectile across Mach, angle of attack, and aerodynamic roll angle. CFD flow solvers Cart3D and CFD^{++} were used to compute and compare the aerodynamic coefficients of the vehicle. In general, Cart3D compared reasonably well for all static aerodynamic coefficients except for pitching moment coefficient. The results showed that modeling viscous effects is necessary to accurately predict the pitching moment coefficient. Since Cart3D is an inviscid flow solver, it is unable to resolve the viscous roll-up of the vortical structures generated along the fin, therefore inaccurately predicting the center of pressure location and leading to incorrect stability predictions for some vehicle orientations. More detail on this research is elaborated in roll-orientation-dependent aerodynamics of a long-range projectile.[31]

4. Conclusion

The prediction accuracy of three numerical methodologies and four aeroprediction codes were investigated. These included Missile DATCOM, Cart3D (flowCart), Kestrel (KCFD, SAMAIR), and CFD++. Four munition configurations were investigated: a generic canard-controlled, subsonic projectile; a long strake-tail missile; a generic ogive-body-tail supersonic missile (AFF); and a generic high-speed configuration (LTV). These analyses were conducted in the interest of evaluating the application of the different methodologies to various munition configurations and flight conditions to better understand their advantages, disadvantages, and constraints. In general, all methodologies generated data with good agreement at low α, low Mach numbers, and roll angles closest to the "+" orientation. All the methodologies showed good agreement beyond these conditions but with additional caveats.

Missile DATCOM was found to be good for predicting longitudinal aerodynamic coefficients, especially at low α. At low Mach numbers, the vortex models in DATCOM predicted some nonlinear flow physics such as vortex fin interaction but failed to make these predictions at higher Mach numbers for a different geometry. This can influence how the center of pressure is calculated, leading to a disagreement in longitudinal aerodynamic coefficients like C_m. However, even at low Mach numbers, there are certain metrics of aerodynamic performance such as roll moment that are not predicted well. But despite disagreement with more sophisticated methods, DATCOM can still predict phenomenon such as roll reversal. DATCOM is also limited in its ability to model vortex shedding on long control surfaces such as strakes. An experimental version of DATCOM was shown to improve these predictions by distributing vorticity shedding chordwise along the strake as opposed to being concentrated at the tip.

The Euler solver (flowCart) in the Cart3D package improves the prediction of aerodynamic coefficients in all ways for a reasonable additional computational cost (minutes instead of seconds). The range of prediction accuracy is increased to moderate angles of attack, $\alpha \approx 15°$. At higher angles of attack, viscous effects of the vortex formation on the leeside of the body become more important and affect the prediction of normal force, center of pressure and, thus, pitching moment. As a Euler code, Cart3D/flowCart cannot accurately predict flow structures dominated by the roll-up within the boundary layer. This includes the initial body vortex rollup and some secondary vortex structures. Yet, it will predict primary vortex structure, especially those shed from relatively sharp wing or fin edges. Despite these limitations, we found Cart3D to be well suited for most of the conditions and for most of the configurations.

The RANS CFD codes Kestrel and CFD^{++} did well predicting the configurations selected in this investigation. However, we have made a note to take proper care in identifying configurations where the codes generate small errors in predicting vortex trajectory and vortex strength, as these small errors may lead to large errors in moments, especially in rolling moment. In the future, we plan to evaluate special cases of these different methodologies and improve our understanding of how best to apply these methodologies and where their weaknesses can be mitigated. A brief description of the computational trade-off in our methodology comparison can be expressed in Table 2. These results are very similar to the table found in *Applied Computational Aerodynamics* by Cummings et al. (p. 47).[32]

Table 2 Hierarchy of computational aerodynamics approaches in this investigation

Computational aerodynamics level	Purpose	Accuracy (avg)	Time to use (including setup)	Strengths	Weaknesses
Engineering method: DATCOM	Forces and moments for conceptual design of large datasets	$\pm 15\%$	Seconds to minutes on a PC	fast	High α, roll moment, vortices at high Mach
Intermediate CFD: Cart3D	Surface pressures, forces, and moments for analysis and design	$\pm 10\%$	Tens of minutes on a PC	Reasonably fast, good prediction low and moderate α	Predictions at high α
CFD methods: CFD^{++} and Kestrel	Detailed flow results (all flow variables throughout the flow field) for analysis	$\pm 5\%$	Hours to weeks on a large computer	Includes most physics, moderate to large α	Time consuming; potential weakness for predicting vortex strength; turbulence model limitations

5. References

1. Rosema C, Doyle J, Blake W. Missile DATCOM user's manual – 2014 revision. Air Force Research Laboratory (US); 2014 Dec. Report No.: AFRL-RQ-WP-TR-2014-0281.

2. Rosema CC, Doyle JB. Fin-shed vortex modeling within missile DATCOM. 49th AIAA Aerospace Sciences Meeting with New Horizons Forum and Aerospace Exposition; 2011 Jan.

3. Doyle JB, Rosema CC. Vortex modeling improvements within missile DATCOM 2014. Army Aviation and Missile Research, Development, and Engineering Center (US); 2016 May. Report No.: RDMR-SS-15-29.

4. Auman LM, Kirby-Brown K. MissileLab user's guide. Army Aviation and Missile Research, Development, and Engineering Center (US); 2012 Oct. Report No.: RDMR-SS-12-08.

5. Aftosmis MJ, Berger MJ, Adomavicius G. A parallel multilevel method for adaptively refined Cartesian grids with embedded boundaries. 38th AIAA Aerospace Sciences Meeting and Exhibit; 2000.

6. Aftosmis MJ, Nemec M, Cliff SE. Adjoint-based low-boom design with Cart3D. 29th AIAA Applied Aerodynamics Conference; 2011 June 27–30.

7. Metacomp Technologies, Inc. CFD^{++} user manual; 2017.

8. Menter FR. Two-equation eddy-viscosity turbulence models for engineering applications. AIAA Journal. 1994;32(8):1598–1605.

9. McDaniel DR, Tuckey TR. HPCMP CREATE^{TM}-AV Kestrel new and emerging capabilities. 2020 AIAA Science and Technology Forum. Paper No.: AIAA-2020-1525; 2020 Jan.

10. Meakin R, Atwood C, Hariharan N. Development, deployment, and support of a set of multi-disciplinary, physics-based simulation software products. 2011 AIAA Science and Technology Forum. Paper No.: AIAA-2011-1104; 2011 Jan.

11. McDaniel DR, Nichols RH, Eymann TA, Starr RE, Morton SA. Accuracy and performance improvements to Kestrel's near-body flow solver. 2016 AIAA Science and Technology Forum. Paper No.: AIAA-2016-1051; 2016 Jan.

12. Eymann TA, Nichols RH, McDaniel DR, Tuckey TR. Cartesian adaptive mesh refinement with HPCMP CREATE-AV Kestrel solver. 2015 AIAA Science and Technology Forum. Paper No.: AIAA-2015-0040; 2015 Jan.

13. Shafer TC, Forsythe, JR, Hallissy BP, Hine DH, Eymann TA. Applications of HPCMP CREATE-AV Kestrel v5 with Cartesian adaptive mesh refinement. 2015 AIAA Science and Technology Forum. Paper No.: AIAA-2015-1040; 2015 Jan.

14. Spalart P, Allmaras SR. A one-equation turbulence model for aerodynamic flows. 1992 AIAA Science and Technology Forum. Paper No.: AIAA-92-0439; 1992 Jan.

15. Vasile JD. Effect of tail fin geometry on the induced roll of a canard-controlled, subsonic projectile. 2019 AIAA Science and Technology Forum. Paper No.: AIAA-2019-0598; 2019 Jan.

16. Vasile JD, Fresconi F, Celmins I, Nelson B. Aerodynamic design optimization of control mechanisms for a subsonic, small diameter munition. AIAA/ASCE/AHS/ASC Structures, Structural Dynamics, and Materials Conference. Paper No.: AIAA 2018-1654; 2018 Jan.

17. Dey S, Aubry RM, Karamete BK, Mestreau EL. Capstone: a geometry-centric platform to enable physics-based simulation and system design. Computing in Science & Engineering. 2016;18(1):32–39.

18. Hine D, Forsythe J, Green BE, Hallissy BP, Lynch E, Shafer T. CREATE-MG capstone version 5 applications. 54th AIAA Aerospace Sciences Meeting. Paper No.: AIAA 2016-1052; 2016 Jan.

19. Allen JM. Aerodynamics of an axisymmetric missile concept having cruciform strakes and in-line tail fins from Mach 0.60 to 4.63. National Aeronautics and Space Administration; 2005 Mar. Report No.: NASA TM-2005-213541.

20. Rosema CC, Abney E, Westmoreland S, Moore H. A comparison of predictive methodologies for missile configurations with strakes. 2015 AIAA Science and Technology Forum. Paper No.: AIAA-2015-2588; 2015 June.

21. Doyle JB, Paul J, DeSpirito J, Anderson M, McGowan G, Smith A, Lesieutre DJ, Ghantous J, Mendenhal MR. Results of the missile and projectile aeroprediction discussion group case study. 2020 AIAA Science and Technology Forum. Paper No.: AIAA-2020-1992; 2020 Jan.

22. Dupuis AD, Hathaway W. Aeroballistic range tests of the basic finner reference projectile at supersonic velocities. Defense Research Establishment; 1997 Aug. Report No.: DREV-TM-9703.

23. Dupuis A. Aeroballistic range and wind tunnel tests of the basic finner reference projectile from subsonic to high supersonic velocities. Defense R&D Canada Valcartier; 2002 Oct. Report No.: TM 2002-136.

24. Dupuis AD, Hathaway W. Aeroballistic range tests of the Air Force finner reference projectile. Defense R&D Canada Valcartier; 2002 May. Report No.: TM 2002-008.

25. West KO. Comparison of free flight spark range and wind tunnel test data for a generic missile configuration at Mach numbers from 0.6 to 2.5. Air Force Armament Laboratory; 1981 Oct. Report No.: AFATL-TR-81-87.

26. West KO, Whyte RH. Free flight and wind tunnel test of a missile configuration at subsonic and transonic Mach numbers with angles of attack up to 30 degrees. 11th Navy Aeroballistic Symposium; 1978 Aug.

27. Bhagwandin VA. High-alpha prediction of roll damping and magnus stability coefficients for finned projectiles. J Spacecraft and Rockets. 2016 July–August;53:4.

28. Kumar RKS, Kumar R, DeSpirito J. Experimental and numerical investigation of the vortex asymmetry on the basic finner configuration. 2021 AIAA Science and Technology Forum; 2021 Jan.

29. Vasile JD, Bryson JT, Gruenwald BC, Fairfax LD, Strohm LS, Fresconi FE. A multi-disciplinary approach to design long range guided projectiles. 2020 AIAA Science and Technology Forum. Paper No.: AIAA-2020-1993; 2020 Jan.

30. Vasile JD, Bryson JT, Fresconi FE. Aerodynamic design optimization of long range projectiles using missile DATCOM. 2020 AIAA Science and Technology Forum. Paper No.: AIAA-2020-1762; 2020 Jan.

31. Vasile JD, Sahu J. Roll orientation-dependent aerodynamics of a long-range projectile. DEVCOM Army Research Laboratory (US); 2020 Aug. Report No.: ARL-TR-9017.

32. Cummings RM, Mason WH, Morton SA, McDaniel DR. Applied computational aerodynamics: a modern engineering approach. Cambridge University Press; 2015 Apr. p. 47; Table 2.1.

Nomenclature

α	=	angle of attack
α_T	=	total angle of attack
C_A	=	axial force coefficient
C_D	=	drag force coefficient
C_L	=	lift force coefficient
C_N	=	normal force coefficient
$C_{N_{NR}}$	=	normal force coefficient in the non-rolled frame
C_m	=	pitching moment coefficient
$C_{m_{NR}}$	=	pitching moment coefficient in the non-rolled frame
C_l	=	rolling moment coefficient
C_p	=	pressure coefficient
δ	=	deflection
δ_q	=	canard deflection for pitching maneuver
δ_p	=	canard deflection for rolling maneuver
d	=	vehicle diameter
L	=	vehicle length
M_∞	=	Mach number
ϕ	=	vehicle roll angle

List of Symbols, Abbreviations, and Acronyms

2D	two-dimensional
3D	three-dimensional
AFF	Air Force Finner Missile
AMR	adaptive mesh refinement
ARL	Army Research Laboratory
CFD	computational fluid dynamics
CFL	Courant–Friedrichs–Lewy
CREATE	Computational Research and Engineering Acquisition Tools and Environments
DEVCOM	US Army Combat Capabilities Development Command
DOD	US Department of Defense
DSRC	DOD Supercomputing Resource Center
HPC	High Performance Computing
L	length
LTV	Laboratory Technology Vehicle
NASA	National Aeronautics and Space Administration
NB	near body
OAL	overall length
RANS	Reynolds–Averaged Navier–Stokes
SST	Shear–Stress Transport
WT	wind tunnel

1 (PDF)	DEFENSE TECHNICAL INFORMATION CTR DTIC OCA
1 (PDF)	DEVCOM ARL FCDD RLD DCI TECH LIB
3 (PDF)	DEVCOM ARL FCDD RLW WD J PAUL J VASILE J DE SPIRITO